Supplementary material for "Subducted Seamounts Beneath the Central Cascadia Forearc" by Trehu, Blakely and Williams.

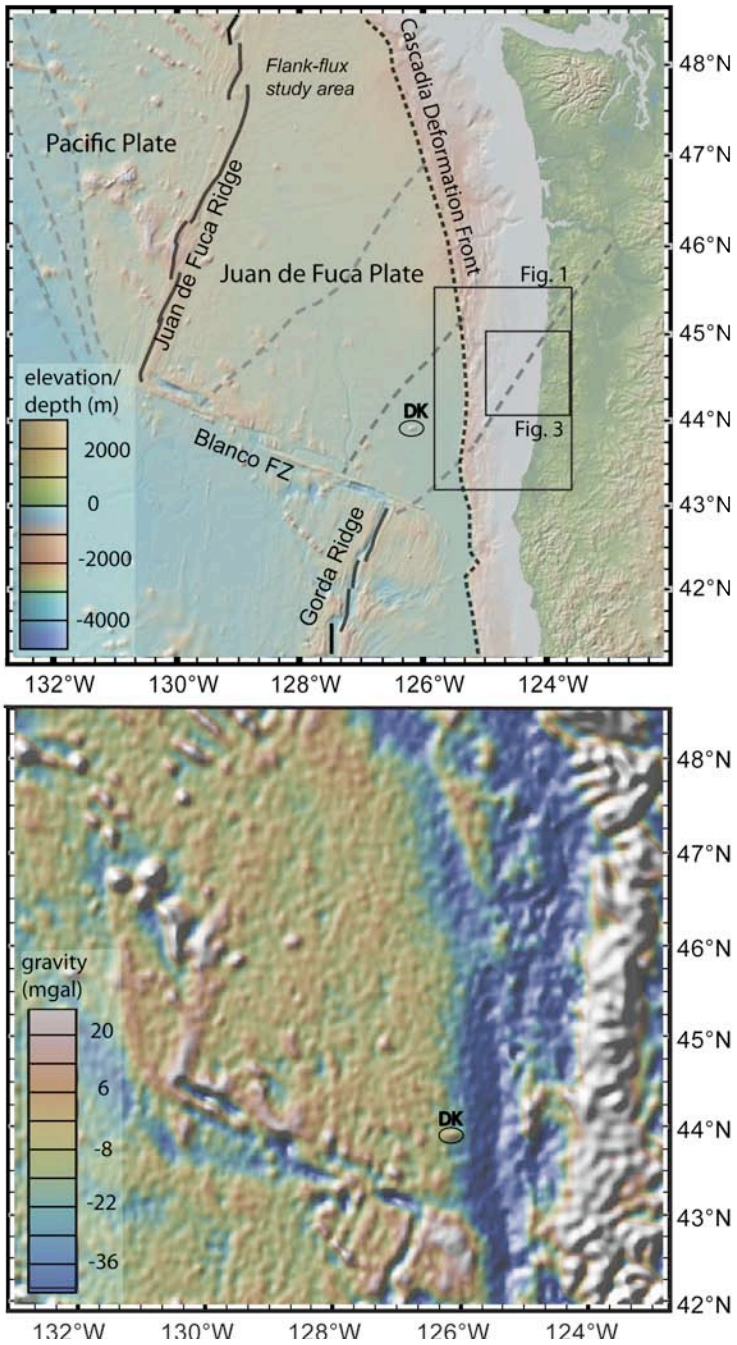

Figure DR1. Bathymetry (top) and gravity anomalies (bottom) of the Juan de Fuca plate (GMRT model 2.0 and Sandwell and Smith model V18.1 accessed via GeoMapApp in May, 2011). This is a larger version of the index map in the corner of Figure 1. The location of the maps in Figures 1 and 3 are shown as is the location of Diebold Knoll (DK).

Figure DR2. Aeromagnetic anomalies in the region covered by Figure 1. The position of the line used to mark the seaward edge of massive Siletz terrane is shown. It is based on the maximum horizontal gradient of the pseudogravity anomaly (Wells et al., 1998) and is ambiguous north of 45°00'N and south of 43° 15'N.

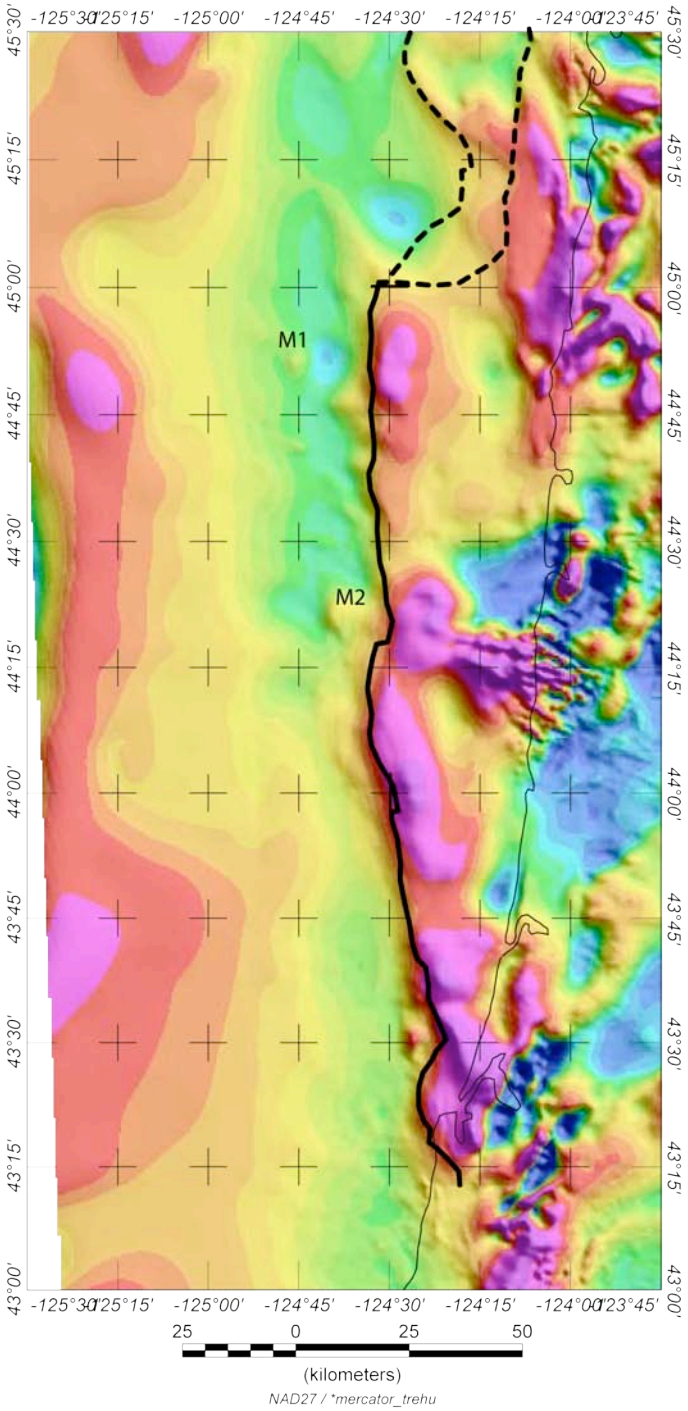

Figure DR3. Seismic reflection data from the slope basin showing the change in onlap patterns with time as the basin filled. The bottom simulating reflection (BSR) labeled on the East end of the transect is the downdip segment of a very strong BSR underlain by very low velocity, gas-charged sediments (see Trehu et al., 1995 for a detailed discussion of this part of the profile). The BSR continues upslope as a strong reflection until it reaches the seafloor in ~500 m of water, where seafloor vent communities have been observed (Torres et al., 2009). Observations of strong BSRs and seafloor vents at the updip limit of the hydrate stability boundary are unusual in Cascadia and are likely a result of uplift in response to seamount subduction.

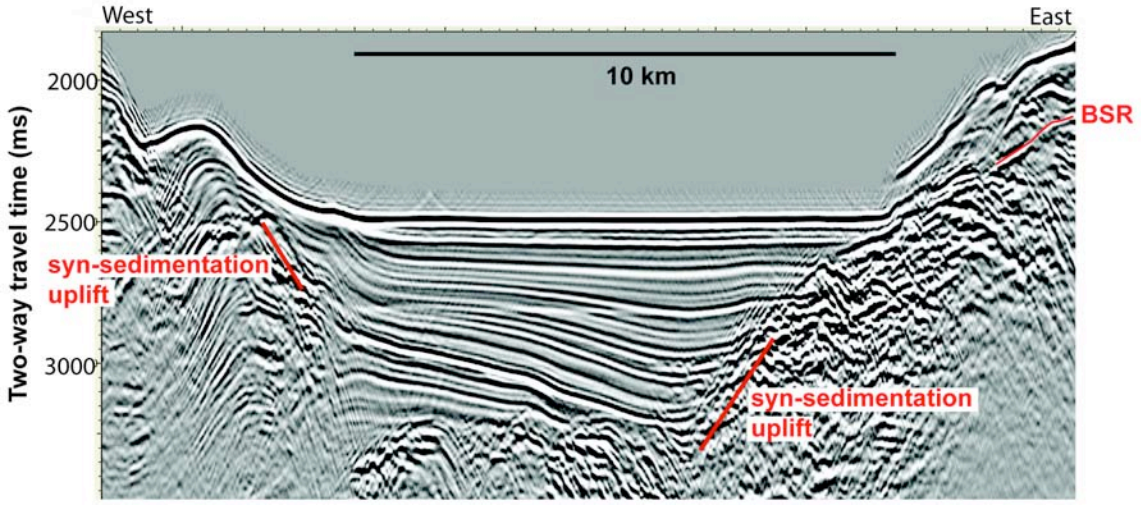

Figure DR4. Starting model for the inversion. This 2D model was derived from arrivals recorded on ocean bottom and land seismographs from airgun shots on an EW line near 44°40'N (Gerdom et al., 2000), corresponding to Y = 67 km. The 2D model was gridded and projected to the north and south. The 1D starting model correspond to the velocity vs. depth function at X = 30 km in the 2D model.

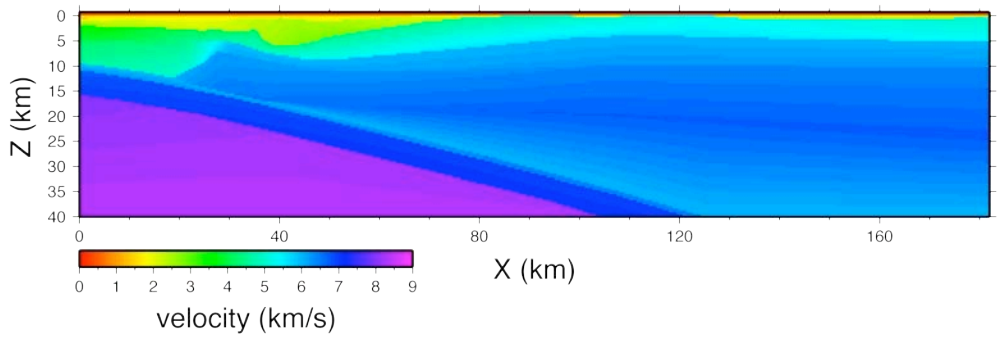

Figure DR5. Slices through the 3D tomographic model. Coastline is near X = 60 km. Black lines show locations of shots and black dots are receivers that were deployed during the 1996 GEOMAR/USGS/OSU ORWELL experiment and were used for this model. White dots are earthquake hypocenters. 4398 travel time picks were inverted using FAST (Zelt and Barton, 1998). Grid spacing was 0.4 km for ray tracing and 2 km for inversion. The solution converged rapidly, as shown in Figure DG6.

The last panel in this composite shows a slice at 11 km depth when the 1D model was used as a starting model. Although this model shows high velocities at relatively shallow depth, it is important to note that the eastward dip of the slab in the 2D starting model is based in primarily on wide-angle reflections from the Moho of the Juan de Fuca plate, which are not first arrivals and were not included in this inversion. The solution of the 1D model is not compatible with the wide-angle second arrivals; first arrivals alone do not constrain the dip of the Juan de Fuca plate. Nevertheless, the 1D inversion also indicates that velocities of ~5.5 km/s extend further east in the northern part of the study area, similar to the result of the inversion that started with the 2D model. The inversion starting with the 2D model also converges to a model that fits the same 4398 travel time picks with misfit of 0.17 s and chi^2 of 2.9, compared to a misfit of 0.27 s and chi^2 of 7.3 for the solution starting with a 1D model.

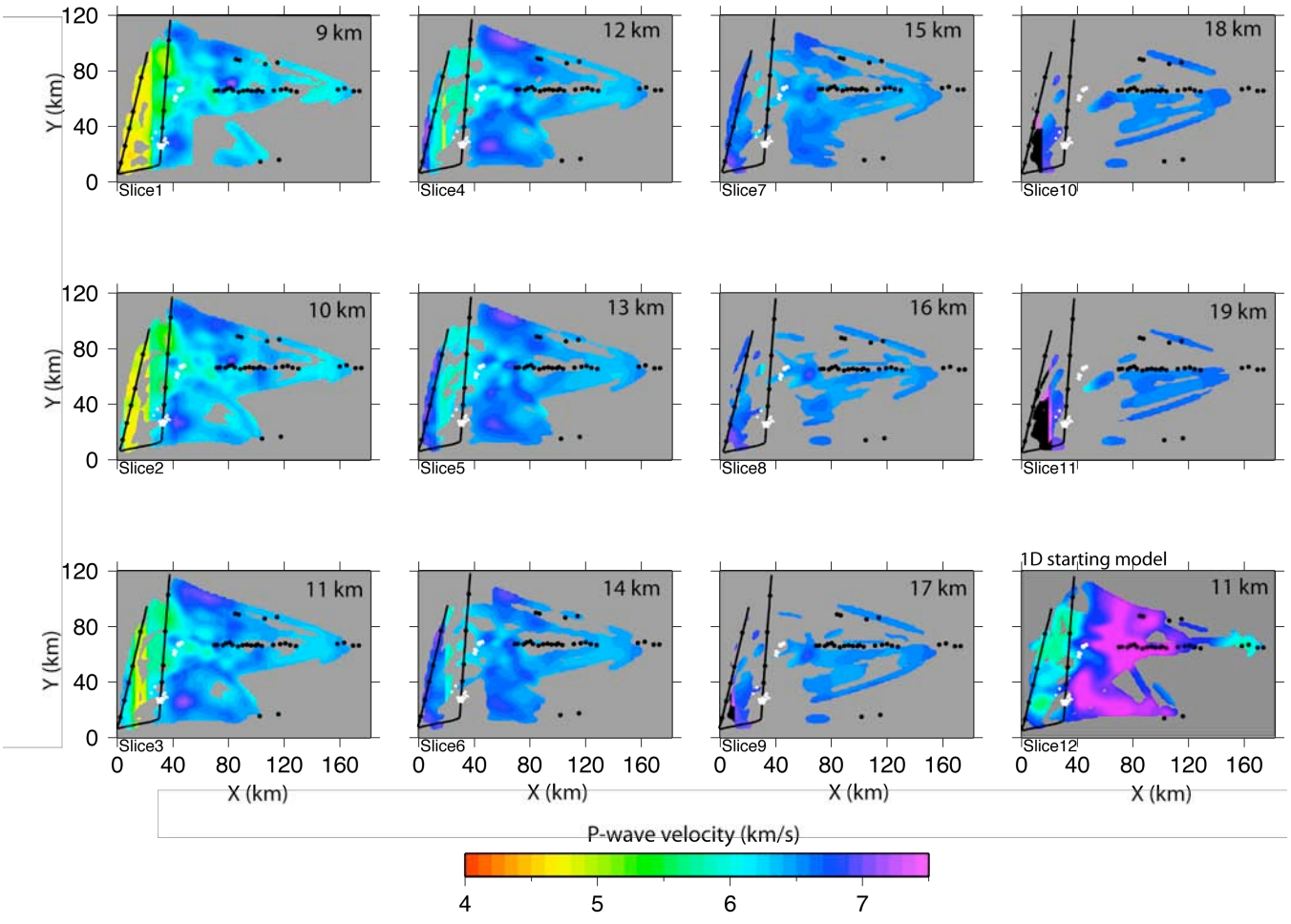

Figure DR6. Root mean squared misfit between observed and calculated travel times, in ms, versus iteration number for the 1D and 2D starting models.

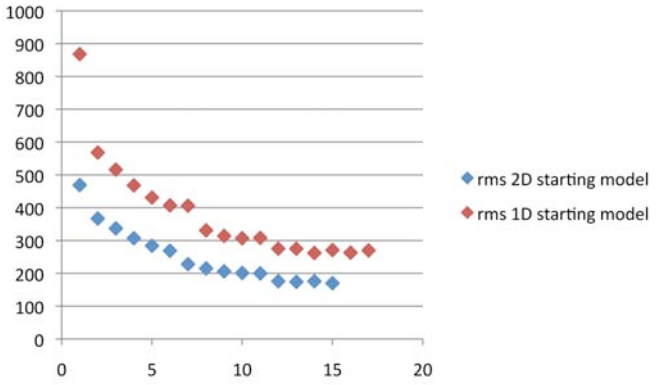

Figure DR7. Examples of large aperture data recorded at Station 18 (large red dot) from Lines 7 and 8. Pg arrival times were used for the inversion. PmP is interpreted to be the wide-angle reflection from the Moho of the Juan de Fuca plate. PiP is a reflection from within the lower crust. Pn is not observed from the fan shots. Amplitudes of PmP are qualitatively consistent with a low velocity subduction channel immediately above the subducting plate in the northern part of the study region because these reflections are observed as strong secondary arrivals at offsets of 80-120 km in the north but not in the south.